[3]Dowell, E. H., "Panel Flutter: A Review of the Aeroelastic Stability of Plates and Shells," *AIAA Journal*, Vol. 8, No. 3, 1970, pp. 385–399.
[4]Bismarck-Nasr, M. N., "Finite Element Analysis of Aeroelasticity of Plates and Shells," *Applied Mechanics Reviews*, Vol. 45, No. 12, Pt. 1, 1992, pp. 461–482.
[5]Bismarck-Nasr, M. N., "Finite Elements in Aeroelasticity of Plates and Shells," *Applied Mechanics Reviews*, Vol. 49, No. 10, Pt. 2, 1996, pp. S17–S24.
[6]Dowell, E. H., "Nonlinear Oscillations of a Fluttering Plate II," *AIAA Journal*, Vol. 5, No. 10, 1967, pp. 1856–1862.
[7]Morino, L., "A Perturbation Method for Treating Nonlinear Panel Flutter Problems," *AIAA Journal*, Vol. 7, No. 3, 1969, pp. 405–411.
[8]Fung, Y. C., "Two-Dimensional Panel Flutter," *Journal of the Aerospace Sciences*, Vol. 25, No. 3, 1958, pp. 145–159.
[9]Han, A. D., and Yang, T. Y., "Nonlinear Panel Flutter Using High Order Triangular Finite Elements," *AIAA Journal*, Vol. 21, No. 10, 1983, pp. 1453–1461.
[10]Mei, C., and Wang, H. C., "Finite Elements Analysis of Large Amplitude Supersonic Flutter of Panels," *Proceedings of the International Conference on Finite Element Methods*, Gordon and Breach, New York, 1982, pp. 944–951.
[11]Novozhilov, V. V., *Foundations of the Nonlinear Theory of Elasticity*, Graylock Press, Rochester, NY, 1953.
[12]Bismarck-Nasr, M. N., "Analysis of Cylindrically Curved Panels Based on a Two Field Variable Variational Principle," *Applied Mechanics Reviews*, Vol. 46, No. 11, Pt. 2, 1993, pp. 571–578.
[13]Bismarck-Nasr, M. N., "Supersonic Panel Flutter Analysis of Shallow Shells," *AIAA Journal*, Vol. 31, No. 7, 1993, pp. 1349–1351.
[14]Bismarck-Nasr, M. N., *Structural Dynamics in Aeronautical Engineering*, AIAA Education Series, AIAA, Reston, VA, 1999.

A. M. Baz
Associate Editor

Compact Schemes with Spatial Filtering in Computational Aeroacoustics

E. K. Koutsavdis,* G. A. Blaisdell,† and A. S. Lyrintzis‡
Purdue University, West Lafayette, Indiana 47907-1282

Introduction

COMPUTATIONAL aeroacoustics (CAA) is concerned with the accurate prediction of small-amplitude acoustic fluctuations and their correct propagation to the far field. In that respect, CAA poses significant challenges for researchers in that the computational scheme should have high accuracy, good spectral resolution, and low dispersion and diffusion errors. Several schemes have been used to satisfy these criteria. An overview of them can be found in Ref. 1. However, two schemes have appeared to capture significant attention lately. Tam and Webb's[2] dispersion relation preserving scheme, which is based on the minimization of the integrated phase errors in the wave number domain, is one such effort. The scheme, explicit in nature, has proven to be a good solution tool. On the other hand, Lele[3] developed a family of high-order spatially implicit schemes, the compact schemes, a subset of which is the well-known Padé approximations. These schemes, which have been used in CAA in the past, have shown that they require few points per wavelength, which results in lower computational requirements. Furthermore, compact schemes resolve well a large portion of the wave number spectrum.

Received 5 November 1998; revision received 12 July 1999; accepted for publication 20 July 1999.

*Graduate Research Assistant, School of Aeronautics and Astronautics. Student Member AIAA.
†Associate Professor, School of Aeronautics and Astronautics. Senior Member AIAA.
‡Associate Professor, School of Aeronautics and Astronautics. Associate Fellow AIAA.

Besides the stringent requirements on the numerical scheme that were mentioned in the preceding paragraph, the accurate and robust calculation of sound depends heavily on the elimination of any sound waves that could result from reflections of the computed sound waves from the computational boundaries. Many researchers have developed nonreflecting or absorbing boundary conditions for CAA. These boundary conditions should allow both the acoustic fluctuations and the hydrodynamic fluctuations to exit the computational domain, without unwanted reflections. Notably Tam and Webb,[2] Thompson,[4] and Giles[5] have developed nonreflecting boundary conditions. A review of the various possible approaches to the problem can be found in Ref. 6.

Because high-order finite difference schemes do not always resolve effectively the high-wave-number range, filters could be introduced to filter out unwanted high-frequency oscillations that may develop. Lele[3] developed a family of seven-point, pentadiagonal compact spatial filters. These filters have been used in large eddy simulations.[7] Visbal and Gaitonde[8] have used a tridiagonal set of these filters as an alternative to artificial dissipation in computational fluid dynamics calculations of unsteady vortical flows. It is indicated in Ref. 8 that filtering is superior to artificial dissipation.

The use of filtering in CAA has been sparse. For example, explicit spatial filtering is used by Hu[9] in conjunction with a seven-point, fourth-order central scheme, with one-sided differences at the boundary, for numerical stabilization and high-frequency wave damping in CAA with the perfectly matched layer boundary conditions. However, the effect of filtering for CAA calculations has not been adequately studied; this is the main objective of the current Note. The filters and the filtering strategies developed in Ref. 8 are used here. We discuss the savings in CPU time that can be achieved with the use of spatial filtering, as opposed to using higher grid resolutions. A more detailed version of our work can be found in Ref. 10.

Numerical Techniques

A sixth-order compact finite difference scheme[3] with fourth-order-explicit, one-sided finite differences at the boundaries is used. A standard fourth-order Runge–Kutta scheme is used for time advancement. This scheme is coupled with an eighth-order compact filter.[8] Furthermore, Tam and Webb's[2] nonreflecting boundary conditions are used.

One- and two-dimensional linearized Euler equations (LEE) and Euler equation solvers based on the techniques mentioned earlier were developed. Benchmark CAA cases[1] were chosen.

Results and Discussion

LEE Results

Because of space limitations, only two-dimensional results are shown here. For the LEE equations, an initial value problem (Ref. 1, Category III) was chosen. This test case consists of a combination of acoustic, entropy, and vorticity pulses on a freestream of Mach number $M_x = 0.5$ in the positive x direction. The results compared well with the analytical solution for a 200×200 uniform mesh and a time step $\Delta t = 0.125$, with no spatial filtering.[10] A calculation on a coarser grid, 120×120, is shown here to demonstrate the effects of filtering. Higher resolution is required for the useful prediction of the propagation of the acoustic waves. At $t = 75$ the right-going acoustic wave has exited the right boundary because it propagates with a speed $c(M_x + 1)$. The left-going wave, propagating with speed $c(M_x - 1)$, has not exited the left boundary. Oscillations emanating from the boundary as a combined result of a low-order boundary closure and the coarseness of the grid travel upstream (Fig. 1). These oscillations, called q waves,[11] then reflect from the left boundary and grow in amplitude, corrupting the solution with high-frequency components. The use of spatial filtering produces significantly improved results. There is a slight reduction (about 1.5%) of the peak amplitude, and some oscillations remain. This filtering operation added only an additional 18% in terms of computational cost. We have found that a grid of 150×150 points still does not eliminate the problem if filtering is not applied.[10] Numerical experiments showed that for this problem a 240×240 size grid is required. However, if a 150×150 grid is used with filtering, then all of the numerical

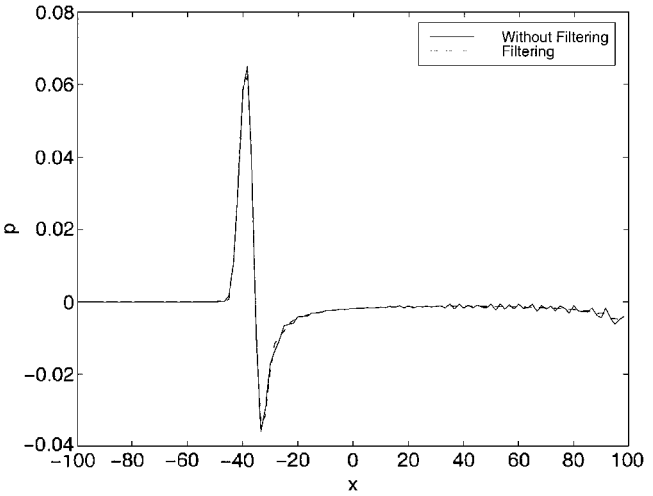

Fig. 1 Pressure plot with and without filtering: grid size 120 × 120 at $t = 75$.

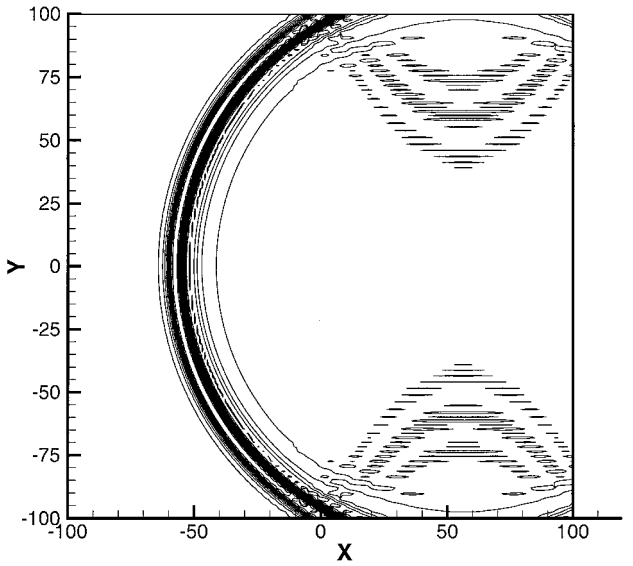

Fig. 2 Pressure contours without filtering: grid size 200 × 200 at $t = 112.5$.

oscillations are eliminated. Thus, utilizing filtering yields substantial CPU savings through the use of coarser grids.

A grid stretched in the y direction was also tried. The stretching function used is the following:

$$y = y_c\left\{1 + \frac{\sinh[\tau(\eta - B)]}{\sinh(\tau B)}\right\} \tag{1}$$

where

$$B = \frac{1}{2\tau}\ln\left(\frac{1 + (e^{\tau} - 1)(y_c/H)}{1 + (e^{-\tau} - 1)(y_c/H)}\right) \tag{2}$$

and $y_c = 100$. The parameter $\tau \in [0, \infty)$ controls the amount of stretching. A value of $\tau = 5$ was used in the calculations. The grid is stretched near both the upper and the lower boundaries.

A pressure contour plot for $t = 112.5$ without filtering is shown in Fig. 2. The wave has been allowed to move out of the right boundary. No reflections are observed from that boundary because the grid is uniform in the x direction and the grid resolution is fine enough to capture the wave. However, a numerical reflection is observed from the bottom and the top boundaries. The reason for the reflection is that the grid, being stretched in the y direction, has an inadequate local grid density near the upper and the lower boundaries, where the local density is defined as $H/\mathrm{d}y_i$ (where $\mathrm{d}y_i$ is the local grid increment and H the height of the domain). In our case $H = 200$. In the areas close to the boundaries, this local grid density is reduced

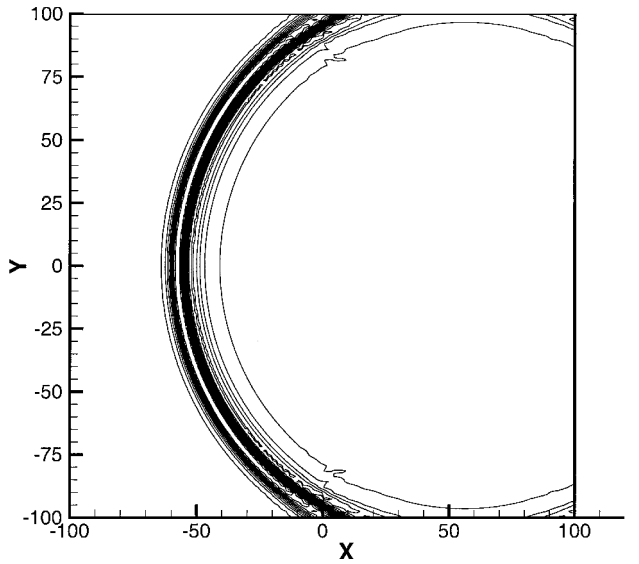

Fig. 3 Pressure contours with filtering: grid size 200 × 200 at $t = 112.5$.

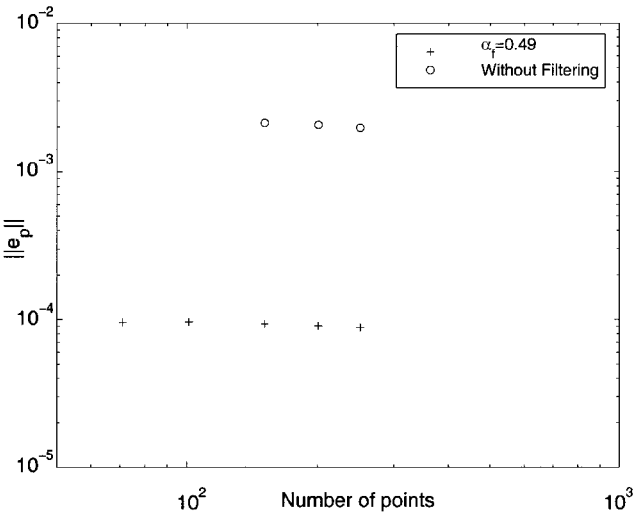

Fig. 4 Error estimate as a function of grid size and filtering.

to about 80 points, that is, the equivalent uniform density being 80 × 80. This low local grid resolution, combined with the fact that the boundary closure scheme is only fourth-order accurate, results in errors during the integration of the boundary conditions. These errors appear as considerable reflections, the amplitude of which exceeds 5%. This can be alleviated using filtering, as shown in Fig. 3. Therefore, filtering again can be used to mitigate the effects of low local resolution. Note that one-dimensional test cases also showed that, for a reasonably stretched grid, the inadequate grid density creates problems and not the grid stretching per se.[10]

Euler Results

For the two-dimensional Euler equations, a weakly nonlinear Gaussian pulse was chosen as the initial condition.[1] To evaluate the performance of the scheme with and without spatial filtering, as well as the boundary conditions, $p - p_{\mathrm{av}}$ was evaluated as an error estimate, where p_{av} is the average pressure in the domain. This was based on the fact that, after the wave leaves the domain, the pressure field should be uniform. Several uniformly spaced grids were used.

Figure 4 summarizes the behavior of the two-dimensional Euler simulation as the grid is refined in terms of the magnitude of the rms error. Note that we are always considering an equal number of points in the x and y directions, and so the horizontal axis indicates the number of points in each direction. The lack of filtering results in high-amplitude, high-frequency numerical oscillations that contaminate the pressure field.[10] This is indicated by the large value of the

error for the results without filtering. Filtering decreases the amount of error by more than an order of magnitude with a comparatively small increase in computational time.

It is also evident that even very coarse grids (for example, a 70×70 grid) with filtering can outperform a dense grid (for example, a 250×250 grid) without filtering. The effect of filtering appears to be more significant than for the linear cases shown. Note that the error reduces very slowly as the grid is refined. As a check, the Euler code was run with a very-small-amplitude initial disturbance. For this case, which is in the linear regime, the error drops in accord with the fourth-order accuracy of the boundary conditions. However, for the nonlinear case shown here (Fig. 4), the drop is much slower (almost zeroth order). This implies that for nonlinear waves the order of the Tam and Webb[2] boundary conditions is reduced, as expected by the far-field assumption used.

Results from the solution of nonlinear Euler equations on nonuniform meshes (not shown here) show behavior similar to those of the LEE discussed.

Conclusions

A filtering strategy for improving CAA computations is demonstrated in this Note. Benchmark cases were chosen for the one- and two-dimensional LEE and full Euler equations. The results confirm that compact finite difference schemes satisfy the stringent requirements of CAA on accuracy and dispersion and diffusion errors.

Filtering appears to be an important tool in CAA. Because it suppresses the unwanted q waves, it can be used as an alternative to grid refinement. Filtering adds only an 18% additional computational cost. It was found that, to get the same quality results without filtering, a substantial increase in CPU time is needed. We also found that it enhances the stability of the numerical method and the boundary conditions.

Finally, stretched-grid studies showed that spurious oscillations arise due to inadequate local grid resolution, as opposed to errors due to variable mesh spacing.

Acknowledgments

This work was sponsored by the NASA John H. Glenn Research Center at Lewis Field under Grant NAG3-2095. J. R. Scott served as the Technical Monitor.

References

[1]Hardin, J. C., Ristorcelli, J. R., and Tam, C. K. W. (eds.), "ICASE/LARC Workshop on Benchmark Problems in Computational Aeroacoustics," NASA CP-3300, May 1995.

[2]Tam, C. K. W., and Webb, J. C., "Dispersion-Relation-Preserving Finite Difference Schemes for Computational Aeroacoustics," *Journal of Computational Physics*, Vol. 107, Aug. 1993, pp. 262–281.

[3]Lele, S. K., "Compact Finite Difference Schemes for Computational Aeroacoustics," *Journal of Computational Physics*, Vol. 103, Jan. 1992, pp. 16–42.

[4]Thompson, K. W., "Time Dependent Boundary Conditions for Hyperbolic Systems," *Journal of Computational Physics*, Vol. 68, Jan. 1987, pp. 1–24.

[5]Giles, M. B., "Nonreflecting Boundary Conditions for Euler Equation Calculations," *AIAA Journal*, Vol. 28, No. 12, 1990, pp. 2050–2058.

[6]Tam, C. K. W., "Advances in Numerical Boundary Conditions for Computational Aeroacoustics," AIAA Paper 97-1774, Jan. 1997.

[7]Spyropoulos, E. T., and Blaisdell, G. A., "Evaluation of the Dynamics Model for Simulations of Compressible Decaying Isotropic Turbulence," *AIAA Journal*, Vol. 34, No. 5, 1996, pp. 990–998.

[8]Visbal, M. R., and Gaitonde, D. V., "High Order Accurate Methods for Unsteady Vortical Flows on Curvilinear Meshes," AIAA Paper 98-0131, Jan. 1998.

[9]Hu, F. Q., "Application of PML Absorbing Boundary Conditions to Benchmark Problems of Computational Aeroacoustics," *Proceedings of the Second Computational Aeroacoustics (CAA) Workshop on Benchmark Problems*, NASA CP-3352, 1996, pp. 119–151.

[10]Koutsavdis, E. K., Blaisdell, G. A., and Lyrintzis, A. S., "On the Use of Compact Schemes with Spatial Filtering in Computational Aeroacoustics," AIAA Paper 99-0360, Jan. 1999.

[11]Vichnevetsky, R., "Invariance Theorems Concerning Reflection at Numerical Boundaries," *Journal of Computational Physics*, Vol. 63, No. 2, 1986, pp. 268–282.

P. J. Morris
Associate Editor

Drag Reduction with a Sliding Wall in Flow over a Circular Cylinder

Byunggwi Choi* and Haecheon Choi†
Seoul National University,
Seoul 151-742, Republic of Korea

Introduction

A NEW idea for reducing skin-friction drag by introducing a passively moving (sliding) belt that replaces the rigid wall in a turbulent boundary layer was presented by Bechert et al.[1] Their basic idea is to release the no-slip condition by implementing a moving wall that is driven by the flow shear stress itself. Thus, the control device does not require any input power, and it is a purely passive device. They implemented a sliding belt in their oil channel. The sliding belt reduced the velocity difference between the mean flow and the wall and reduced the skin friction by 9%. It was shown that the measured belt velocity varied between 6 and 12% of the centerline velocity, depending on the belt tension. Issues related to the implementation of the sliding belt are addressed in detail by Bechert et al.[1]

An idea similar to that of Bechert et al.[1] may be applied to bluff-body problems such as flow over a circular cylinder to reduce the form drag. That is, implementing the moving wall, which is passively driven by the wall shear stress, on a part of the cylinder surface increases the momentum nearby. The increased momentum near the wall may be large enough to overcome the adverse pressure gradient formed at the rear part of the cylinder and to delay the separation, resulting in the form-drag reduction. This concept is tested in the present study by numerical simulations.

Sliding Wall

Figure 1 shows a schematic of the sliding-belt device installed in a circular cylinder to realize the sliding-wall concept. The belts are located on the upper and lower parts of the cylinder surface. Here θ' and γ denote the front location and length of the sliding belt, respectively. The total shear force exerted on the lower sliding belt is

$$F = (1 - \mu_s) \int_A \tau \, \mathrm{d}A = ma \tag{1}$$

where m is the mass of the belt, a the acceleration, τ the flow shear stress, μ_s the friction coefficient between the belt and pulley, and A the area of the belt surface. The flow shear stress τ on the belt is written in cylindrical coordinates (r, θ) as

$$\tau = \mu \left(\frac{\partial u_\theta}{\partial r} - \frac{u_\theta}{R} \right)_{r=R} \tag{2}$$

where u_θ is the velocity in the azimuthal direction, R is the radius of the cylinder, and μ is the viscosity.

From Eqs. (1) and (2), the acceleration of the lower belt can be obtained as

$$a = \frac{\mathrm{d}u_w}{\mathrm{d}t} = \alpha \left(R \overline{\left. \frac{\partial u_\theta}{\partial r} \right|_{r=R}} - u_w \right) \tag{3}$$

where u_w is the belt (sliding-wall) velocity, $\alpha = (1 - \mu_s)\mu A / mR$, and an overbar denotes the spatial averaging over the lower sliding belt. Note that $u_w = \bar{u}_\theta|_{r=R}$ for the lower belt and $u_w = -\bar{u}_\theta|_{r=R}$ for the upper belt (Fig. 1). Equation (3) is numerically integrated in time to obtain the time sequence of the lower-belt velocity. The velocity of the upper belt can be similarly obtained.

Received 8 March 1999; revision received 19 October 1999; accepted for publication 2 November 1999.

*Graduate Student, School of Mechanical and Aerospace Engineering.

†Associate Professor, School of Mechanical and Aerospace Engineering; choi@socrates.snu.ac.kr. Member AIAA.